Near-inertial waves on the "nontraditional" β plane

T. Gerkema[1]
Laboratoire des Ecoulements Geophysique, Grenoble, France

V. I. Shrira
Department of Mathematics, Keele University, Keele, UK

Received 4 June 2004; revised 29 September 2004; accepted 18 November 2004; published 18 January 2005.

[1] Propagation of linear near-inertial waves on the β plane is considered, taking into account the horizontal component of the Earth's rotation, $\tilde{f}$. (Terms, effects etc., due to this component will be referred to as "nontraditional," for brevity.) It is shown that the combined effect of β and $\tilde{f}$ changes the dynamics in a fundamental way. For a vertically unbounded domain, an exact solution shows that near-inertial waves can pass through the inertial latitude, unlike under the traditional approximation. For parameter values typical of the ocean, the subinertial domain extends several hundreds of kilometers poleward of the inertial latitude. The solution undergoes a profound change if a vertically bounded, instead of unbounded, domain is considered. Part of the wave energy then accumulates at the poleward end of the subinertial domain, which involves an evolution toward infinitesimal horizontal and vertical scales. For vertically nonuniform stratification, examined here using the Garrett-Munk exponential profile, one finds a wedge-like waveguide, which becomes increasingly narrow in the poleward direction, and drives subinertial waves into the region of the weakest stratification, i.e., the abyss. For typical parameters, the relative amount of poleward traveling energy that gets trapped is estimated to lie between 10 and 30%; its dependence on latitude and stratification is also outlined. The observational evidence and possible implications for abyssal mixing are discussed.

Citation: Gerkema, T., and V. I. Shrira (2005), Near-inertial waves on the ''nontraditional'' β plane, *J. Geophys. Res.*, *110*, C01003, doi:10.1029/2004JC002519.

1. Introduction

[2] Near-inertial internal waves are a ubiquitous phenomenon in the ocean, and the inertial peak usually dominates the internal-wave spectrum [*Fu*, 1981]. They are thought to be mostly generated by atmospheric disturbances; a global map of the input of near-inertial energy has recently been constructed [*Alford*, 2003].

[3] The theoretical description of the propagation of near-inertial waves involves two subtleties which set it apart from the rest of the internal-wave spectrum: the β effect and the "nontraditional" effect. Since the wave-frequency σ lies close to f, one finds that $\sigma/f - 1$ varies noticeably, even over short distances (i.e., distances over which f as such varies relatively little); thus the β effect plays a crucial role [e.g., *Munk*, 1980; *Garrett*, 2001]. The "nontraditional" terms, i.e., the terms due to the horizontal component of the Earth's rotation ($\tilde{f}$), modify the dynamics of near-inertial waves in two ways. First, they create a class of subinertial internal waves [e.g., *LeBlond and Mysak*, 1978; *Brekhovskikh and Goncharov*, 1994] that does not exist under the so-called "traditional approximation," i.e., if one assumes $\tilde{f} = 0$. Second, they produce a nonvanishing horizontal group velocity at the inertial frequency [*Badulin et al.*, 1991]. In a recent study [*Gerkema and Shrira*, 2004], transitions between the superinertial and subinertial classes were shown to be a generic phenomenon for near-inertial waves propagating in a horizontally inhomogeneous fluid; here we will consider the specific case of the inhomogeneity due to β.

[4] The combined effect of β and $\tilde{f}$ has been explored in an implicit way in studies on internal-wave propagation in spherical shells [*Friedlander and Siegmann*, 1982; *Dintrans et al.*, 1999]. These studies revealed the existence of solutions that involve wave trapping poleward of the inertial latitude. The oceanographic relevance and possible implications for abyssal mixing were noticed by *Maas* [2001]. However, owing to the complexity of the full spherical geometry, it has remained impossible to disentangle the mechanism involved in this trapping, and to pinpoint the roles of β, $\tilde{f}$, and the geometry. Moreover, no estimates were made of the portion of energy that gets trapped this way, which is essential for judging the oceanographic significance of this mechanism.

[5] In this paper we will derive a tractable equation that combines the nontraditional effects with the β effect, in its

[1]Now at Royal Netherlands Institute for Sea Research, Den Burg (Texel), Netherlands.

0148-0227/05/2004JC002519$09.00

most reduced form, and enables us to describe the trapping, linking it firmly to the simultaneous effect of β and $\tilde{f}$. The derivation of the equation is the subject of section 2. (We should note at the outset that we exclude the equatorial region, for which the dynamics of near-inertial waves requires a separate treatment [see *Maas*, 2001, and references therein].) In section 3, we summarize some known results on the dynamics on the nontraditional f plane, and show how the energy properties differ from those obtained under the traditional approximation. In addition to the "traditional" class of superinertial waves, there is now a class of subinertial waves. The β effect enables the transition from one class to another, as is shown in sections 4.1 and 4.2. In a vertically bounded domain, one finds an additional feature: wave-trapping in the subinertial domain (remainder of section 4). Observational evidence of nontraditional effects is discussed in section 5.

2. Derivation of the Governing Equation

[6] We start with the linearized momentum equations on the nontraditional β plane, under the Boussinesq approximation, along with the continuity and (reduced) energy equations,

$$u_t - fv + \tilde{f}w = -p_x, \tag{1a}$$

$$v_t + fu = -p_y, \tag{1b}$$

$$w_t - \tilde{f}u = -p_z + b, \tag{1c}$$

$$u_x + v_y + w_z = 0, \tag{1d}$$

$$b_t + N^2 w = 0, \tag{1e}$$

where p is the perturbation pressure divided by a constant reference density, and b denotes the buoyancy. A Cartesian frame is used with the coordinates x (west-east), y (south-north), and z (vertical, positive upward); u, v, and w are the corresponding velocity components. We allow the buoyancy frequency N to depend on z (unless stated otherwise). In the traditional approximation, one would take $\tilde{f} = 0$ [*Eckart*, 1960].

[7] On the nontraditional β plane, the parameter f varies linearly with the meridional coordinate ($f = f_0 + \beta y$), while $\tilde{f}$ is kept constant to ensure that vorticity and angular momentum principles remain valid [*Grimshaw*, 1975]. The constants $\tilde{f}$, f_0, and β are defined in the usual way,

$$\left(\tilde{f}, f_0\right) = 2\Omega\left(\cos\phi, \sin\phi\right); \beta = 2\Omega\cos\phi/R,$$

where ϕ denotes a fixed latitude, Ω is the Earth's angular velocity, and R is the Earth's radius.

[8] The effects of a zonal dependence are discussed separately, in Appendix A; in the remainder, we will consider plane waves propagating in the meridional direction, so that $\partial/\partial x = 0$. We will look for time periodic solutions, and write $u = U(y, z)\exp i\sigma t$ (similarly for the other fields). Under these assumptions, (1a)–(1e) can be reduced to an equation for V, the meridional velocity component,

$$\left(N^2 - \sigma^2 + \tilde{f}^2\right)V_{yy} + 2f\tilde{f}V_{yz} - \left(\sigma^2 - f^2\right)V_{zz} + \tilde{f}\beta V_z = 0. \tag{2}$$

The y-dependent f occurs in the second and third term. The horizontal scales we will consider are much smaller than R, so we can in the second term approximate f by f_0 (except in equatorial regions, which we exclude here). In the third term, however, the β-effect matters even at small scales, because σ is very close to f_0; here we retain the leading-order term in β,

$$\sigma^2 - f^2 \approx \sigma^2 - f_0^2 - 2f_0\beta y. \tag{3}$$

With these approximations, (2) becomes

$$AV_{yy} + 2BV_{yz} + (C + 2f_0\beta y)V_{zz} + \tilde{f}\beta V_z = 0, \tag{4}$$

where $A = N^2 - \sigma^2 + \tilde{f}^2$, $B = f_0\tilde{f}$, and $C = f_0^2 - \sigma^2$; B and C are constants, while A may depend on z, via N. The traditional approximation would remove the second and fourth term ($B, \tilde{f} = 0$). Equation (4), which unifies nontraditional effects with the β effect, forms the starting point of further study in this paper. (We note that (4) could also have been obtained without initially assuming f to be constant, since arguments similar to those used to approximate (2) by (4) would have allowed us to neglect variations in $\tilde{f}$.) First, we will briefly consider the case $\beta = 0$, and discuss results that serve as a preparation for later sections.

3. The f Plane

[9] Taking $\beta = 0$ in (4) leads us back to the nontraditional f plane; the characteristics are then given by

$$\frac{dz}{dy} = \frac{B \pm (B^2 - AC)^{1/2}}{A} \equiv \mu_{\pm}. \tag{5}$$

For simplicity, we will assume N to be constant (N_c). The condition of hyperbolicity, $B^2 - AC > 0$, delineates the range of allowable frequencies σ; hence one obtains the lower and upper bounds, $\sigma_{\min}$ and $\sigma_{\max}$,

$$\sigma_{\min}^2,\ \sigma_{\max}^2 = s \mp \left[s^2 - (f_0 N_c)^2\right]^{1/2}, \tag{6}$$

with $2s = N_c^2 + f_0^2 + \tilde{f}^2$. These expressions were earlier derived by *Brekhovskikh and Goncharov* [1994]; an alternative but equivalent form is given by *LeBlond and Mysak*, [1978]. The horizontal component $\tilde{f}$ enlarges the frequency domain at both ends; in particular, if $N_c > |f_0|$ (as is usually the case in the ocean), one finds a lower bound $\sigma_{\min} < |f_0|$ instead of the "traditional" lower bound $|f_0|$; there is now a class of subinertial internal waves: $\sigma_{\min} < \sigma < |f_0|$.

[10] A schematic view of the characteristics $\xi_{\pm} = \mu_{\pm}y - z$ in the three frequency regimes (superinertial, inertial, and subinertial) is shown in Figure 1 (in each, we assume $A > 0$, a condition normally satisfied in the ocean); they indicate the direction of energy-propagation. As is discussed by *Badulin et al.* [1991], the (horizontal) group velocity does not vanish at the inertial frequency, unlike under the traditional approximation. Further insight into the properties of near-inertial waves can be obtained from the expressions for kinetic and potential energy (E_k, E_p), derived in Appen-

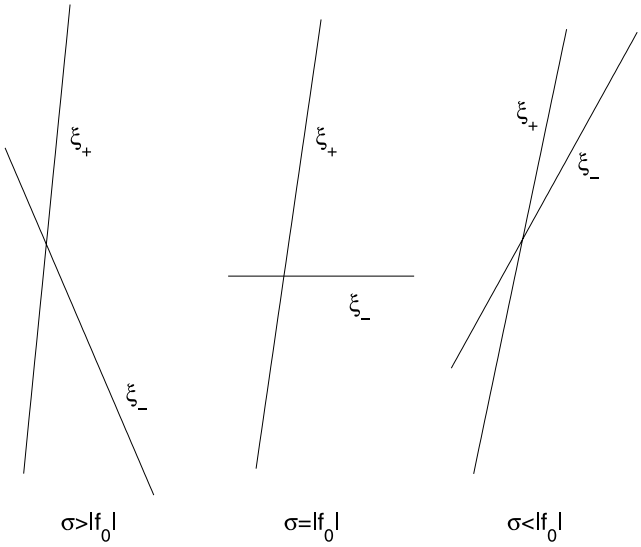

Figure 1. Schematic view of the characteristics $\xi_{\pm} = \mu_{\pm} y - z$ on the "nontraditional" f plane, given by (5), for the three regimes: superinertial, inertial, and subinertial. The poleward direction is to the right.

dix B. In Figure 2 we plot the ratios E_p/E_k and $E_{k,u}/E_{k,v}$, as functions of wave-frequency σ. With $\tilde{f}$ included, we have to distinguish the plus-branch (thick solid line) and the minus-branch (dotted line), associated with $\mu_{\pm}$ in (5). Under the traditional approximation, by contrast, the two coincide (thin line), since then $\mu_+^2 = \mu_-^2$. In the near-inertial range, the nontraditional plus-branch has a much larger E_p/E_k ratio than the traditional branch (Figure 2a). Importantly, at $\sigma = |f_0|$ the horizontal polarization is noncircular for the plus-branch (Figure 2b). Other aspects of internal waves on the nontraditional f plane (like modal solutions, reflection at slopes, etc.) are discussed elsewhere [*Gerkema and Shrira*, 2004].

4. The β Plane

[11] For $\beta \neq 0$ and a fixed near-inertial frequency σ, we can place the inertial latitude at $y = 0$, so that $|f_0| = \sigma$ and $C = 0$; this involves no loss of generality. Equation (4), with $C = 0$, will be our starting point for studying near-inertial waves on the nontraditional β plane.

4.1. Inertial and Turning Latitudes

[12] We first reconsider the meaning of the inertial latitude. Under the traditional approximation, it acts as a turning latitude, in the sense of the classical turning point in the WKB description [e.g., *Munk*, 1980; *Garrett*, 2001]. However, if one includes $\tilde{f}$, then near-inertial waves can exist as subinertial waves poleward of the inertial latitude. This can be seen by considering the characteristics corresponding to (4), given by

$$\frac{dz}{dy} = \frac{B \pm (B^2 - A(C + 2f_0\beta y))^{1/2}}{A}. \tag{7}$$

As noted above, we can assume $C = 0$. For constant N the characteristics can be found in explicit form (see section 4.3), but we first consider the general case $N(z)$,

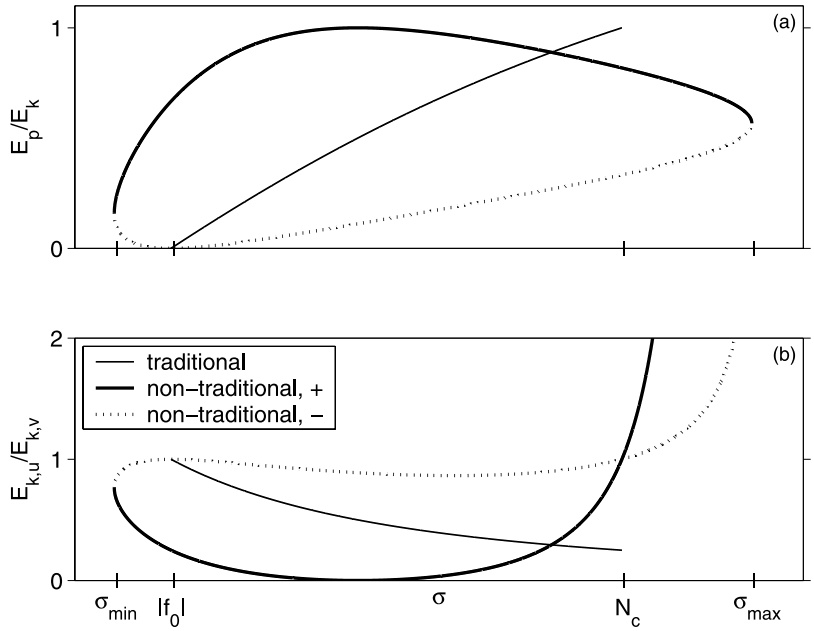

Figure 2. Ratios of energies as a function of wave-frequency σ: (a) the ratio of potential and kinetic energies, and (b) the ratio of the two horizontal kinetic energies. In both panels, thick (solid and dotted) lines represent expressions obtained without the traditional approximation; thin lines represent expressions obtained with the traditional approximation. In nontraditional dynamics, the window of allowable frequencies is bounded by $\sigma_{\min}$ and $\sigma_{\max}$, which are the roots of $B^2 - AC = 0$. Under the traditional approximation, these bounds become $|f_0|$ and N_c. Parameter values are $N_c = 2|f_0|$ and $\phi = 45°$N.

hence $A(z)$. The curve separating the hyperbolic and elliptic regimes is found by requiring the argument of the square root in (7) to be zero,

$$y = \frac{B^2}{2f_0\beta A(z)} = \frac{f_0 \tilde{f} R}{2\left(N(z)^2 - f_0^2 + \tilde{f}^2\right)}. \tag{8}$$

Under the traditional approximation ($\tilde{f}$, $B = 0$), this curve forms a vertical straight line, $y = 0$, irrespective of the profile of $N(z)$; this means that the inertial latitude here always acts as a turning latitude.

[13] If the traditional approximation is abandoned, two cases have to be distinguished, since there is now a dependence on N. For constant $N = N_c$, the curve (8) still forms a vertical straight line,

$$y = y_* \equiv \frac{f_0 \tilde{f} R}{2\left(N_c^2 - f_0^2 + \tilde{f}^2\right)}. \tag{9}$$

Hence we can still speak of a turning latitude, understood as the boundary of wave propagation, but it now lies poleward of the inertial latitude. (We assume here that $A > 0$, a condition that is almost always satisfied in the ocean.) In the region between the inertial and turning latitudes, the waves are subinertial. Since the horizontal scales considered here are small compared to R, expression (9) is practically equivalent to the exact one derived by *Hughes* [1964] [see also *LeBlond and Mysak*, 1978, equation (10.26)], which was obtained without recourse to the β plane approximation. In using the term "turning" latitude for $y = y_*$, we should add the caveat that the behavior at this latitude can be quite unlike that under the traditional approximation; in fact, one finds that in a vertically bounded domain, subinertial waves accumulate (rather than turn) at the deepest point at $y = y_*$ (see section 4.3).

[14] For nonconstant N, we can no longer speak of a turning latitude, since the curve (8) no longer forms a vertical line. The curve extends to a certain limiting latitude $y_{\max}$, whose value is found by calculating y in (8) for $\min(N(z))$. This case will be illustrated in section 4.4. If $N(z)$ has more than one local minimum, each of them will have its own corresponding value of $y_{\max}$.

4.2. Unbounded Domain, Constant *N*

[15] The ideas discussed in the previous section can be illustrated by considering a simple solution of (4) for a vertically unbounded domain, with constant $N = N_c$. Substituting $V = \Theta(y)\exp\, im(z - By/A)$ into (4), with $C = 0$, gives

$$\Theta'' - \hat{m}^2[y - y_c]\Theta = 0, \tag{10}$$

where $\hat{m}^2 = 2f_0\beta m^2/A$, and

$$y_c = y_* + \frac{i\tilde{f}}{2f_0 m}, \tag{11}$$

whose real part, y_*, is given by (9). (The results obtained below do not noticeably change if one ignores the imaginary term in (11); it is indeed plausible that the term is always negligible for realistic parameters, but we will not pursue this point here.) Equation (10) can be solved in terms of Airy functions (with complex argument): $\Theta = \mathrm{Ai}(\hat{m}^{2/3}[y - y_c])$. Hence V becomes, if we take the imaginary part,

$$V = \Im\left\{\mathrm{Ai}\left(\hat{m}^{2/3}[y - y_c]\right)\, \exp im(z - By/A)\right\}. \tag{12}$$

We can arbitrarily superpose solutions with different values of m; an example is shown in Figure 3b; for comparison we show in Figure 3a the same solution but under the traditional approximation (i.e., taking $\tilde{f} = 0$ in (12)). These figures illustrate the point, discussed above, that the inertial latitude no longer acts as a turning latitude if the traditional approximation is abandoned: While superinertial waves reflect at the inertial latitude ($y = 0$) in Figure 3a, they pass it unhindered in Figure 3b, become subinertial, and finally reflect at $y = y_*$(= 136 km), the real turning latitude. The structure of the field in Figure 3b indicates that there are two ways to pass the inertial latitude: horizontally via a parabolically shaped curve, or diagonally via a steep rectilinear curve. This will be confirmed below when we consider the characteristics.

[16] The solution (12) represents a direct generalization of known solutions, also in terms of Airy functions, obtained earlier under the traditional approximation [*Munk*, 1980]. In contrast to the latter case, there is now no straightforward way to use (12), or more general solutions in which m is allowed to be complex, as a starting point for obtaining solutions in a vertically bounded domain. This difficulty is due to the nonseparable character of the problem, and reflects the profound change brought about in the solution if one changes the configuration from vertically unbounded to bounded. As we will suggest below on the basis of characteristics, part of the energy of the near-inertial waves then accumulates at the "turning" latitude y_*, at the bottom.

4.3. Bounded Domain, Constant *N*

[17] For constant $N = N_c$ the explicit form of the characteristics can be found from (7)

$$\xi_\pm = \frac{B}{A}y \mp \frac{1}{3f_0\beta A^2}\left(B^2 - 2f_0\beta A y\right)^{3/2} - z. \tag{13}$$

The characteristic coordinates allow us to reduce (4) to its canonical form; if we ignore the last term in (4), the resulting form is the Euler-Poisson-Darboux equation,

$$6\left(\xi_+ - \xi_-\right)V_{\xi_+\xi_-} = V_{\xi_+} - V_{\xi_-}.$$

Although the general solution of this equation is known [*Darboux*, 1915], the problem of finding a solution satisfying the boundary conditions in a vertically bounded domain has not yet been solved.

[18] Returning to the characteristics (13), and making the Taylor expansion around $y = 0$, we find that in the vicinity of the inertial latitude, ξ_+ and ξ_- take a linear and parabolic form, respectively (leaving out the constants),

$$\xi_+ = -z + \frac{2B}{A}y + O\left(y^2\right); \qquad \xi_- = -z + \frac{f_0\beta}{2B}y^2 + O\left(y^3\right).$$

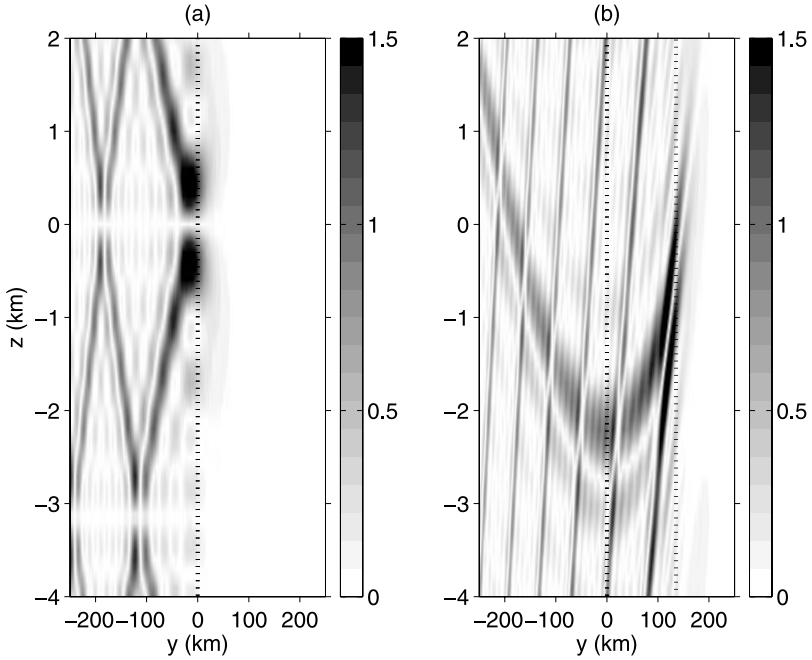

Figure 3. Meridional velocity component $|V|$ of near-inertial waves in a vertically unbounded domain, constructed by superposing solutions (12) for $m = 1,\cdots,5$. The waves are superinertial for $y < 0$ and subinertial for $y > 0$; the poleward direction is to the right. (a) Under the traditional approximation: $\tilde{f} = 0$; here the inertial and turning latitudes coincide at $y = 0$. (b) Without the traditional approximation; now the turning latitude lies at $y_* = 136$ km, i.e., poleward of the inertial latitude $y = 0$. In both panels, parameter values are $N_c = 5 \times 10^{-4}$rad s^{-1}, $\phi = 45°$N, $\sigma = f_0$.

These shapes are already recognizable in Figure 3b; locally, they are also consistent with the behavior on the nontraditional f plane, shown schematically in Figure 1.

[19] We now consider a vertically confined domain, and take a starting point at the left end (in the superinertial domain); see Figure 4. The thick lines represent the nontraditional characteristics (13). Given the separation of scales (i.e., the waves are short compared to β^{-1}), we will adopt a WKB-approach: We will assume that the wave energy propagates along the characteristics and that no internal reflections occur. The parabolic-shaped ξ_- then shows how the wave energy enters the subinertial domain, and how, after reflection at the turning latitude, the energy will continue to propagate along the steep ξ_+ characteristic. Until here, the pattern is identical to that in Figure 3b. The difference starts when the ξ_+ characteristic encounters the bottom, and reflects. The alternation between ξ_+ and ξ_- characteristics then leads to an accumulation of energy in the lower corner at the turning latitude. This is in stark contrast with the pattern under the traditional approximation (i.e., (13) with $\tilde{f} = 0$), where the waves reflect at the inertial latitude (thin lines).

[20] The trapped solution shown in Figure 4 also indicates that the horizontal and vertical scales become infinitely short at the turning latitude. This is what one would expect on the basis of the theory of the nontraditional f plane; for a vertically bounded domain, *Saint-Guily* [1970] showed that the waves become infinitely short at the minimum frequency. (This subinertial short-wave limit is discussed in more detail by *Gerkema and Shrira* [2004].) The minimum frequency is indeed attained precisely at latitude y_*.

[21] We note that not all energy will get trapped into the corner. Energy that passes the inertial latitude sufficiently shallow via ξ_- will return into the super-inertial domain (via ξ_+). Moreover, energy that passes via ξ_+ will always return into the super-inertial domain (via ξ_-).

4.4. Bounded Domain, Exponential N

[22] For nonconstant stratification $N(z)$, the subinertial waves, which owe their existence to nontraditional effects, are trapped in regions around minima of N [*Brekhovskikh and Goncharov*, 1994, p.256; *Gerkema and Shrira*, 2004]: The more subinertial they become, the closer they must stay near the minimum. This is illustrated in Figure 5 for an exponential profile: $N = N_0\exp(z/b)$, with the standard values $N_0 = 5.24 \times 10^{-3}$rad s^{-1} and $b = 1.3$ km [e.g., *Garrett*, 2001]. The waveguide is delineated by the dotted exponential curve, which represents (8).

[23] The characteristic equations (7) are now solved numerically, because of the vertical dependence of A. As before, we assume $C = 0$; that is, the inertial latitude lies at $y = 0$. The results are shown in Figure 5. Again, one observes the contrasting behavior in the traditional and nontraditional cases (thin and thick lines, respectively). In the former case, the inertial latitude acts as a turning latitude; this is the case considered previously, also in terms of characteristics, by *Garrett* [2001]. In the nontraditional case, by contrast, the inertial latitude becomes transparent, and part of the near-inertial wave energy is guided toward the bottom in the subinertial domain, as shown in Figure 5a; notice the large extent of this domain: nearly 600 km. The end of the waveguide lies at the limiting latitude $y_{\max} = 581$ km (see section 4.1); here the ratio σ/f equals

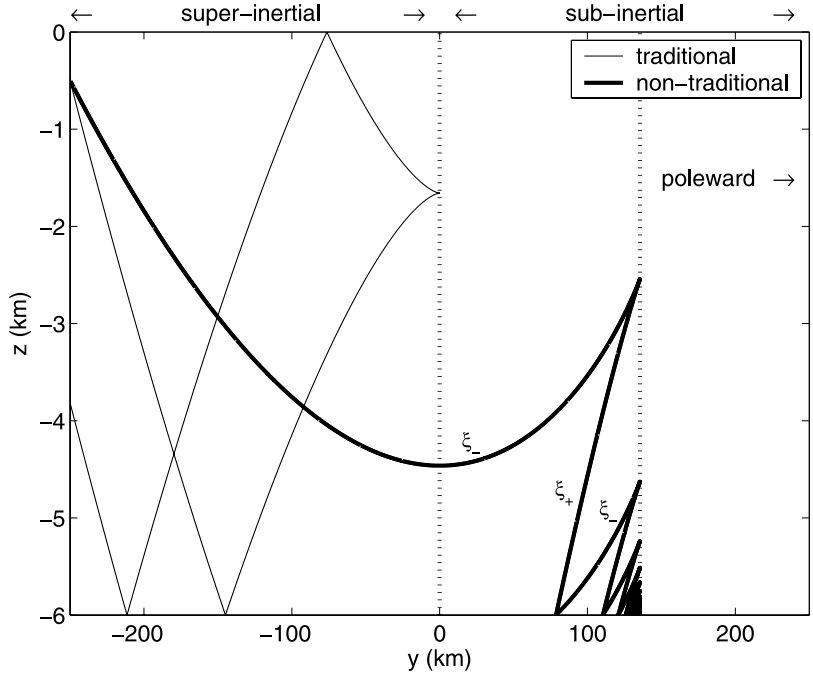

Figure 4. Characteristic curves $\xi_{\pm} = const$, given by (13), in a vertically *bounded* domain. Thin lines: under the traditional approximation ($\tilde{f} = 0$); thick lines: *without* the traditional approximation. In the latter case, waves become trapped at the turning latitude, at the bottom. Parameter values are as in Figure 3.

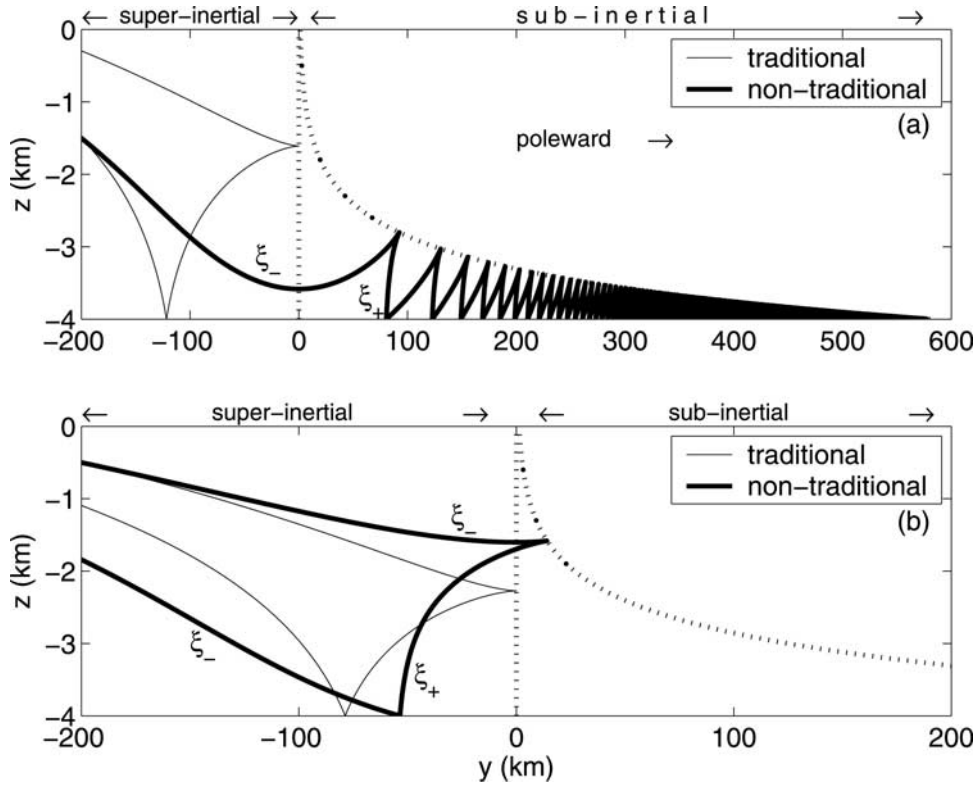

Figure 5. Characteristic curves $\xi_{\pm} = const$, solved numerically from (7) for an exponential profile of $N(z)$. Thin lines: under the traditional approximation ($\tilde{f} = 0$); thick lines: without the traditional approximation. In the latter case, waves can either (a) become abysally trapped at the limiting latitude ($y_{max} = 581$ km) or (b) be reflected back into the superinertial domain. The exponential dotted curve denotes the transition between the hyperbolic and elliptic regimes. As before, $\phi = 45°$N and $\sigma = f_0$.

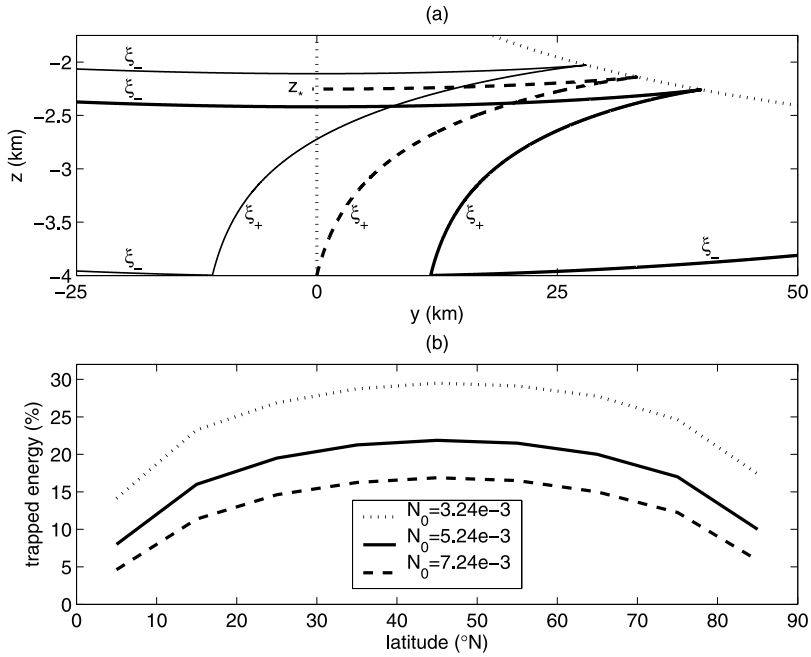

Figure 6. (a) Threshold depth z_* at the inertial latitude, determined by using the ξ_+ characteristic originating from the bottom at the inertial latitude, and the reflected ξ_- (dashed lines). Only energy that enters the subinertial domain via ξ_- at a lower position will become trapped. The thin line shows an example of a return into the superinertial domain; the thick line shows an example of subinertial trapping. Parameters are as in Figure 5. (b) Percentage of trapped energy is shown, as a function of latitude and stratification. Here it is assumed that all ways of passing the inertial latitude are equally likely.

$f_0/(f_0 + \beta y_{\max}) = 0.92$. These subinertial waves would normally still fall within the inertial peak (in observed internal-wave spectra), which has a typical width of $0.1f$.

[24] Whether or not this accumulation toward $y_{\max}$ takes place depends on where and how the wave energy enters the subinertial domain (see section 4.5); an example in which wave energy returns equatorward is shown in Figure 5b. The question of how to estimate the (relative) amount of trapped energy, and its dependence on latitude and stratification, is considered in the following section.

4.5. Trapped Subinertial Energy

[25] In terms of characteristics, there are two ways to pass the inertial latitude: diagonally via ξ_+, or horizontally via ξ_-. To proceed, we will assume that both are equally likely, and that, for each, all heights of passage are also equally likely. It follows from (7) that ξ_- is less steep than ξ_+. Hence a poleward energy flux that passes the inertial latitude via ξ_+ will, after reflection in the subinertial domain, return into the superinertial domain via ξ_- (compare Figure 5b, thick line, and Figure 6a, thin line). Only energy passing via ξ_- can become trapped, if the passage occurs sufficiently deep. The threshold level z_* can be determined as indicated in Figure 6a (dashed line). Energy that enters via ξ_- at a higher level will return into the superinertial domain (thin line in Figure 6a), while for a lower passage the energy cannot escape (thick line in Figure 6a), and will continue to propagate toward the limiting latitude (see Figure 5a, thick line).

[26] As stated above, we assume the incident energy fluxes to be uniformly distributed with depth; hence the portion of trapped energy is given by $(H - z_*)/(2H)$, where H is the water depth. (The amount can never be larger than 50% because the energy entering via ξ_+ does not get trapped.) To get an idea of how large the percentage is for realistic parameters, we use again an exponential profile of N, as in section 4.4. As before, we take $b = 1.3$ km, but we now consider three different values for N_0 to find the dependence on the strength of the stratification. The other key parameter is latitude, and the dependence on both is shown in Figure 6b. The portion of trapped energy is largest at midlatitudes, and becomes (as one would expect) larger for weaker stratification. Overall, it lies roughly between 10 and 30%.

[27] The two key properties of these trapped subinertial waves suggest their potential importance to deep-ocean mixing, and, hence, to large-scale ocean dynamics: the fact that their horizontal and vertical scales become increasingly small as they approach the limiting latitude and the fact that they are trapped in the region of weak stratification, which singles out the abyssal ocean as their habitat.

5. Discussion

[28] We summarize the principal differences between nontraditional ($\tilde{f} \neq 0$) and traditional ($\tilde{f} = 0$) dynamics of near-inertial waves on the β plane, and discuss how nontraditional effects may be detected in observations. The frequency domain is enlarged by including $\tilde{f}$; in particular, a class of subinertial waves exists ($\sigma_{\min} < \sigma < |f_0|$) that disappears under the traditional approximation (section 3,

and references therein). Observationally, this class cannot be expected to form a distinctive feature in internal-wave temporal spectra, because it falls within the inertial peak, which has a typical width of 10% of $|f_0|$.

[29] Superinertial waves propagating toward the equator will move downward via ξ_+ and upward via ξ_- (see Figure 1). According to (B3) in Appendix B, the downward vertical energy flux will then be larger than the upward one. (This asymmetry disappears under the traditional approximation, since the inequality in (B3) then becomes an equality.) Such a vertical asymmetry has indeed been observed by *D'Asaro and Perkins* [1984]. However, a quantitative comparison is hindered by the assumption they made on the conservation of vertical wave number; in nontraditional dynamics the upward and downward propagating beams have different vertical wave numbers. (For example, for reflection at a flat bottom one finds $m_+/m_- = \mu_-/\mu_+$, with $\mu_\pm$ given by (5).)

[30] For near-inertial waves, properties like energy ratios and polarization are strongly modified by nontraditional effects (Figure 2), especially in regions of weak stratification. In particular, these properties are now different for the two characteristics (as indicated by the plus and minus branches in Figure 2). This makes it possible, in principle at least, to infer the direction of propagation (compare Figure 1) from, for example, the polarization of the horizontal velocity field. Under the traditional approximation, the distinction between the two branches disappears. It has been reported that the polarization observed at near-inertial frequencies is often not circular (*Konyaev and Sabinin* [1992] write: "The ratio of the axes of the most intense oscillations at near-inertial frequencies was measured in the MegaPoligon-experiment. The histogram of these ratios is spread between 0.4 to 1, with the maximum in the interval 0.7–0.8, while the frequency histogram is compressed near inertial frequencies (~15%). In other words, the orbits of the most intense inertial oscillations deviate significantly from circular ones.") This fact can be explained by nontraditional theory, but not by traditional theory (Figure 2b).

[31] If one abandons the traditional approximation, the inertial latitude no longer acts as a turning latitude (and for nonconstant stratification, one cannot even speak anymore of a turning latitude): On the nontraditional β plane, freely propagating subinertial waves can exist in a region poleward of the inertial latitude. The extent of this region depends on the stratification, but will typically be on the order of a few hundreds of kilometers in the deep ocean (section 4). As illustrated in Figure 3b, the region is large enough to avoid confusion with the rapidly decaying signal (present beyond the inertial latitude) that one observes under the traditional approximation (Figure 3a).

[32] Even though the subinertial range is large in terms of distance, from the observational perspective one still faces the problem that in terms of frequency, the subinertial range falls under the cloak of the inertial peak. At certain special latitudes, this may pose less of a problem. For example, semidiurnal lunar (M2) internal tides can create waves of half their frequency by parametric subharmonic instability (PSI). This process is at work, in principle, wherever the subharmonics can exist as freely propagating waves. Under the traditional approximation, with its lower bound $|f_0|$ for internal-wave frequencies, one thus finds the latitude 28.8°N/S, equatorward of which PSI can work. In nontraditional dynamics, however, PSI can already work at some distance poleward of this latitude, typically 1° to 5° (depending on the stratification). *Hibiya and Nagasawa* [2004] recently estimated diapycnal diffusivities at various latitudes, and found markedly higher values at lower latitudes, presumably due to PSI. Interestingly, the high values do not start at 28.8°N, but indeed already a few degrees northward of it. If this is due to nontraditional effects, it should start even farther northward at deeper locations (the measurements by *Hibiya and Nagasawa* [2004] were made down to about 1.5 km).

[33] The so-called "critical" (i.e., inertial) latitude for internal tides also deserves special mention; for M2 tides, it lies at 74.5°N/S. According to traditional linear theory, internal tides can neither pass through the inertial latitude nor be generated poleward of it. However, freely propagating internal tides of M2 period have been observed well beyond this latitude, as discussed by *Vlasenko et al.* [2003], who propose an explanation in terms of nonlinear effects and higher harmonics. An alternative explanation, which works also for linear waves, lies in the inclusion of $\tilde{f}$; internal tides can then exist up to several degrees beyond their "critical" latitude.

[34] The more poleward subinertial waves come, the weaker the stratification must be for them to exist (Figure 5a), implying an accumulation of wave energy in the region of weakest stratification, the abyssal ocean. This creates a vertical asymmetry in the distribution of near-inertial wave energy not present under the traditional approximation. Recently, persistent abyssally intensified near-inertial motions have indeed been found in year-long observations [*Van Haren et al.*, 2002], suggesting the presence of an abyssal waveguide, as predicted by nontraditional theory.

[35] This narrowing abyssal waveguide, in which horizontal and vertical scales become increasingly small (Figure 5a), can be expected to be a region of intensified mixing (other mechanisms of abyssal mixing were discussed in a review by *Garrett and St. Laurent* [2002]). Recently, strongly increased abyssal mixing has been reported in the Greenland Sea, just beyond the "critical" latitude for M2 internal tides [*Walter*, 2003]. The depth range in which this strong mixing occurs falls within the scope of the subinertial waveguide, but is smaller; in the absence of detailed measurements on internal waves (or their spectra), the role of subinertial waves must here remain a hypothesis.

[36] We finally note that the inclusion of nontraditional terms in numerical studies should pose no problems. It may often be appropriate to adopt a "quasi-hydrostatic" approach [*White and Bromley*, 1995; *Marshall et al.*, 1997]; that is, one neglects w_t in (1c) but retains the term with f.

Appendix A: Zonal Dependence

[37] Here we discuss the effects of a zonal dependence. For simplicity, we assume N constant (N_c) and consider

waves of the form $u = \hat{u}(y)\exp\, i(kx + mz + \sigma t)$. After substitution into (1a)–(1e), one can reduce the resulting equations to one for the meridional velocity component $\hat{v}$,

$$\left[m^2\left(\sigma^2 - f^2\right) + im\tilde{f}\beta - \left(N_c^2 - \sigma^2\right)\left(k^2 - \beta k/\sigma\right)\right]\hat{v} + 2imf\,\tilde{f}\hat{v}' + \left(N_c^2 - \sigma^2 + \tilde{f}^2\right)\hat{v}'' = 0. \tag{A1}$$

This is a very rich equation that deserves further scrutiny; it includes Rossby waves as well as the whole spectrum of internal inertio-gravity waves, and is nonhydrostatic as well as nontraditional. Here we will only look into the effect of the terms involving k on near-inertial waves. Those terms do not involve $\tilde{f}$, and are, therefore, the same as under the traditional approximation [cf. *Munk*, 1980, equation (13)].

[38] Making the same approximations as in the transition from (2) to (4), and following the procedure of section 4.2, we arrive at the same solution (12) but now with

$$y_c = y_* + \frac{i\tilde{f}}{2f_0 m} - \frac{N_c^2 - \sigma^2}{2f_0\beta m^2}\left(k^2 - \beta k/\sigma\right), \tag{A2}$$

with y_* again given by (9); by convention, the inertial latitude lies at $y = 0$ (i.e., $\sigma = |f_0|$). Assuming $kR \gg 1$, we can approximate $k^2 - \beta k/\sigma$ by k^2; it is then seen from (A2) that the zonal wave number k produces an equatorward shift of the turning latitude, as opposed to the poleward shift produced by the nontraditional contribution y_*. Whereas nontraditional terms also modify the structure of the solution (12), by producing the exponent $-mBy/A$, the terms with k leave the structure unaffected. We may thus conclude that the analysis of the case $k = 0$ in previous sections would, in essence, remain valid if one includes a zonal dependence.

Appendix B: Energetics

[39] We substitute $V = \hat{v}\,\exp\, i(ly + mz + \sigma t)$ with constant $\hat{v}$ (and likewise for the other fields) in (1a)–(1e), with $\beta = 0$, $\partial/\partial x = 0$ and $N = N_c$. One then finds the dispersion relation $l/m = -\mu_\pm$, and

$$E_{k,u} \equiv \hat{u}\hat{u}^* = \sigma^{-2}\left(\tilde{f}\mu_\pm - f_0\right)^2\hat{v}\hat{v}^*; \quad E_{k,v} \equiv \hat{v}\hat{v}^*$$

$$E_{k,w} \equiv \hat{w}\hat{w}^* = \mu_\pm^2\hat{v}\hat{v}^*; \quad E_p \equiv N_c^{-2}\hat{b}\hat{b}^* = \sigma^{-2}N_c^2\mu_\pm^2\hat{v}\hat{v}^*.$$

Hence the total kinetic energy $E_k = E_{k,u} + E_{k,v} + E_{k,w}$.

[40] The components of the group velocity vector $\vec{c}_\pm = (\sigma_{l,\pm},\ \sigma_{m,\pm})$ follow by taking derivatives in the dispersion relation, $l/m = -\mu_\pm$,

$$m^{-1} = -\frac{d\mu_\pm}{d\sigma}\,\sigma_{l,\pm}; \quad -lm^{-2} = -\frac{d\mu_\pm}{d\sigma}\,\sigma_{m,\pm}. \tag{B1}$$

The derivatives of $\mu_\pm$ can be obtained in explicit form, via (5), but are not needed here. Dividing the two expressions gives

$$\frac{\sigma_{l,\pm}}{\sigma_{m,\pm}} = \frac{1}{\mu_\pm}. \tag{B2}$$

We now have the tools to predict what happens when a beam reflects at the bottom, where it changes characteristic (ξ_+ to ξ_-, or vice versa). First of all, the energy flux must remain conserved, i.e., $E_+|\vec{c}_+| = E_-|\vec{c}_-|$. Hence the vertical energy flux must satisfy

$$\frac{E_+\left|\sigma_{m,+}\right|}{E_-\left|\sigma_{m,-}\right|} = \frac{\left|\vec{c}_-\sigma_{m,+}\right|}{\left|\vec{c}_+\sigma_{m,-}\right|} = \frac{\left(\mu_-^{-2} + 1\right)^{1/2}}{\left(\mu_+^{-2} + 1\right)^{1/2}} > 0, \tag{B3}$$

where we used (B2).

[41] **Acknowledgments.** The authors are grateful to Hans van Haren, Uwe Harlander, and Leo Maas for helpful discussions. This work was supported by INTAS 01-0025 and INTAS 01-234.

References

Alford, M. H. (2003), Redistribution of energy available for ocean mixing by long-range propagation of internal waves, *Nature*, *423*, 159–162.

Badulin, S. I., V. M. Vasilenko, and M. I. Yaremchuk (1991), Interpretation of quasi-inertial motions using Megapoligon data as an example, *Izv. Atmos. Oceanic Phys.*, *27*(6), 446–452.

Brekhovskikh, L. M., and V. Goncharov (1994), *Mechanics of Continua and Wave Dynamics*, 342 pp., Springer-Verlag, New York.

Darboux, G. (1915), *Leçons sur la Théorie Générale des Surfaces et les Applications Géométriques du Calcul Infinitésimal*, vol. II, 567 pp., Gauthier-Villars, Paris.

D'Asaro, E. A., and H. Perkins (1984), A near-inertial internal wave spectrum for the Sargasso Sea in late summer, *J. Phys. Oceanogr.*, *14*, 489–505.

Dintrans, B., M. Rieutord, and L. Valdettaro (1999), Gravito-inertial waves in a rotating stratified sphere or spherical shell, *J. Fluid Mech.*, *398*, 271–297.

Eckart, C. (1960), *Hydrodynamics of Oceans and Atmospheres*, 290 pp., Elsevier, New York.

Friedlander, S., and W. L. Siegmann (1982), Internal waves in a rotating stratified fluid in an arbitrary gravitational field, *Geophys. Astrophys. Fluid Dyn.*, *19*, 267–291.

Fu, L. L. (1981), Observations and models of inertial waves in the deep ocean, *Rev. Geophys.*, *19*(1), 141–170.

Garrett, C. (2001), What is the "near-inertial" band and why is it different from the rest of the internal wave spectrum?, *J. Phys. Oceanogr.*, *31*(4), 962–971.

Garrett, C., and L. St. Laurent (2002), Aspects of deep ocean mixing, *J. Oceanogr.*, *58*, 11–24.

Gerkema, T., and V. I. Shrira (2004), Near-inertial waves in the ocean: Beyond the "traditional approximation," *J. Fluid Mech.*, in press.

Grimshaw, R. H. J. (1975), A note on the β-plane approximation, *Tellus*, *27*(4), 351–356.

Hibiya, T., and M. Nagasawa (2004), Latitudinal dependence of diapycnal diffusivity in the thermocline estimated using a finescale parameterization, *Geophys. Res. Lett.*, *31*, L01301, doi:10.1029/2003GL017998.

Hughes, B. (1964), Effect of rotation on internal gravity waves, *Nature*, *201*, 798–801.

Konyaev, K. V., and K. D. Sabinin (1992), *Waves Inside the Ocean* (in Russian), 272 pp., Giidrometeoizdat, St. Petersburg.

LeBlond, P. H., and L. A. Mysak (1978), *Waves in the Ocean*, 602 pp., Elsevier, New York.

Maas, L. R. M. (2001), Wave focusing and ensuing mean flow due to symmetry breaking in rotating fluids, *J. Fluid Mech.*, *437*, 13–28.

Marshall, J., C. Hill, L. Perelman, and A. Adcroft (1997), Hydrostatic, quasi-hydrostatic, and nonhydrostatic ocean modeling, *J. Geophys. Res.*, *102*(C3), 5733–5752.

Munk, W. (1980), Internal wave spectra at the buoyant and inertial frequencies, *J. Phys. Oceanogr.*, *10*, 1718–1728.

Saint-Guily, B. (1970), On internal waves: Effects of the horizontal component of the Earth's rotation and of a uniform current, *Dtsch. Hydrogr. Z.*, *23*(1), 16–23.

Van Haren, H., L. Maas, and H. Van Aken (2002), On the nature of internal wave spectra near a continental slope, *Geophys. Res. Lett.*, *29*(12), 1615, doi:10.1029/2001GL014341.

Vlasenko, V., N. Stashchuk, K. Hutter, and K. Sabinin (2003), Nonlinear internal waves forced by tides near the critical latitude, *Deep Sea Res., Part I*, *50*, 317–338.

Walter, M. (2003), Warming of Greenland Sea Deep Water induced by abyssal mixing, Ph.D. thesis, 134 pp., Univ. of Bremen, Bremen, Germany.

White, A. A., and R. A. Bromley (1995), Dynamically consistent, quasi-hydrostatic equations for global models with a complete representation of the Coriolis force, *Q. J. R. Meteorol. Soc.*, *121*, 399–418.

T. Gerkema, Royal Netherlands Institute for Sea Research, P.O. Box 59, NL-1790 AB Den Burg (Texel), Netherlands. (gerk@nioz.nl)

V. I. Shrira, Department of Mathematics, Keele University, Keele ST5 5BG, UK. (v.i.shrira@maths.keele.ac.uk)